Heat Capacity of a Strongly Interacting Fermi Gas

Joseph Kinast,[1] Andrey Turlapov,[1] John E. Thomas,[1]* Qijin Chen,[2] Jelena Stajic,[2] Kathryn Levin[2]

We have measured the heat capacity of an optically trapped, strongly interacting Fermi gas of atoms. A precise addition of energy to the gas is followed by single-parameter thermometry, which determines the empirical temperature parameter of the gas cloud. Our measurements reveal a clear transition in the heat capacity. The energy and the spatial profile of the gas are computed using a theory of the crossover from Fermi to Bose superfluids at finite temperatures. The theory calibrates the empirical temperature parameter, yields excellent agreement with the data, and predicts the onset of superfluidity at the observed transition point.

Strongly interacting, degenerate atomic Fermi gases (1) provide a paradigm for strong interactions in nature (2). In all strongly interacting Fermi systems, the zero-energy scattering length is large compared with the interparticle spacing, a property that produces universal behavior (3, 4). Predictions of universal interactions and effective field theories in nuclear matter (3, 5–7) are tested by measurements of the interaction energy (1, 8–10). Anisotropic expansion of strongly interacting Fermi gases (1) is analogous to the "elliptic flow" of a quark-gluon plasma (2). High-temperature superfluidity has been predicted (11–16) in strongly interacting Fermi gases, which can be used to test theories of high-temperature superconductivity (17). Microscopic evidence for superfluidity has been obtained by observing the pairing of fermionic atoms (18–20). Macroscopic evidence arises in anisotropic expansion (1) and in collective excitations (21–23).

In superconductivity and superfluidity, measurements of the heat capacity have played an important role in determining phase transitions (24) and in characterizing the nature of bosonic and fermionic excitations. We report on the measurement of the heat capacity for a strongly interacting Fermi gas of ^{6}Li atoms that are confined in an optical trap. Our experiments (25) examine the fundamental thermodynamics of the gas.

Thermodynamic properties of the Bardeen-Cooper-Schrieffer–Bose-Einstein condensation (BCS-BEC) crossover system are computed (26) using a consistent many-body theory (27, 28) based on the conventional mean-field state (29). BCS-BEC crossover refers to the smooth change from the BCS superfluidity of fermions to the BEC of dimers, by varying the strength of the pairing interaction (for example, by tuning a magnetic field). The formalism of (16, 17, 28) was applied recently (30) to explain radio-frequency measurements of the gap (20). The theory contains two contributions to the entropy and energy arising from fermionic and bosonic excitations. The latter are associated principally with excited pairs of fermions (Cooper pairs at finite momentum). In this model, there is no direct boson-boson coupling, and fermion-boson interactions are responsible for the vanishing of the pair chemical potential μ_{pair} in the superfluid regions. The vanishing of μ_{pair} implies that, within a trap, the associated low-temperature power laws in the entropy and energy are the same as those of the homogeneous system (31). This is to be contrasted with models that involve noninteracting bosons and fermions (32). Our BCS-like ground state ansatz will be inapplicable at some point when the fermionic degrees of freedom have completely disappeared and the gas is deep in the BEC regime, where the power laws associated with true interacting bosons are expected (31). In that case, direct interboson interactions must be accounted for, and they will alter the collective-mode behavior (33). However, on the basis of collective-mode experiments (21–23) and their theoretical interpretation (34, 35), one can argue that the BCS-like ground state appears to be appropriate in the near-resonance, unitary regime. The thermodynamic quantities within the trap are computed by using previously calculated profiles (36) of the various energy gaps and the particle density as a function of the radius.

Unlike the pairing gap in the weak-coupling BCS limit, the pairing gap in the unitary regime is very large. Well below the superfluid transition temperature T_c, fermions are paired over much of the trap, and unpaired fermions are present only at the edges of the trap. These unpaired fermions tend to dominate the thermodynamics associated with the fermionic degrees of freedom, and lead to a power law that is higher than linear in the temperature (T) dependence of the entropy. The contribution from finite-momentum Cooper pairs leads to a $T^{3/2}$ dependence of the entropy on temperature. Both bosonic and fermionic contributions are important at low T.

An important feature of these fermionic superfluids is that pair formation occurs at a higher temperature, T^*, than T_c, where pairs condense. At temperatures $T > T^*$, the entropy approaches that of the noninteracting gas. For $T_c < T < T^*$, the attraction is strong enough to form quasi-bound (or preformed) pairs, which are reflected in the thermodynamics. At these intermediate temperatures, a finite energy (i.e., the pseudogap) is needed to create single fermion excitations (16, 17, 28). In the unitary regime, both T^* and T_c are large fractions of the Fermi temperature T_F, signifying high-temperature pair formation and very high-temperature superfluidity.

We prepared a degenerate unitary Fermi gas composed of a 50:50 mixture of the two lowest spin states of ^{6}Li atoms near a Feshbach resonance. To cool the gas, we used forced evaporation at a bias magnetic field of 840 G in an ultrastable CO_2 laser trap (1, 2, 26). After cooling the atoms well into the degenerate regime, energy was precisely added to the trapped gas at fixed atom number. The gas was then allowed to thermalize for 0.1 s, and was released from the trap and imaged at 840 G after 1 ms of expansion to determine the number of atoms and the empirical temperature parameter $\tilde{T}$. For our trap, the total number of atoms was $N = 2.2\ (0.3) \times 10^5$. The corresponding noninteracting gas Fermi temperature was $T_F = (3N)^{1/3}\hbar\overline{\omega}/k_B \approx 2.5\ \mu K$, where $\hbar$ is Planck's constant divided by 2π, $\overline{\omega}$ is the geometric mean of the trap oscillation frequencies, k_B is Boltzmann's constant, and T_F is small compared $U_0/k_B = 35\ \mu K$, where U_0 is the final trap depth.

Energy was precisely added to the trapped gas at fixed atom number by releasing the cloud from the trap and permitting it to expand for a short time $0 \leq t_{heat} \leq 460\ \mu s$, after which the gas was recaptured. Even for a strongly interacting gas, the energy input is well defined for very low initial temperatures, where both the equation of state and the expansion dynamics are known. During the times t_{heat} used in these experiments, the axial size of the gas changed negligibly, whereas transverse dimensions expanded by a factor $b_\perp(t_{heat})$. Therefore, the mean harmonic-trapping potential energy $\langle U_{HO} \rangle$ in each of the two transverse directions increased by a factor $b_\perp^2(t_{heat})$.

The initial potential energy was readily determined at zero temperature from the

[1]Physics Department, Duke University, Durham, NC 27708–0305, USA. [2]James Franck Institute and Department of Physics, University of Chicago, 5640 South Ellis Avenue, Chicago, IL 60637, USA.

*To whom correspondence should be addressed. E-mail: jet@phy.duke.edu

equation of state of the gas, $(1 + \beta)\varepsilon_F(x) + U_{HO} = \mu_0$ (1, 8), where $\varepsilon_F(x)$ is the local Fermi energy as a function of position, β is the unitary gas parameter (1, 3, 6–8), and μ_0 is the global chemical potential. This equation of state is supported by low-temperature studies of the breathing mode (21, 23, 33, 35) and the spatial profiles (1, 6, 36). It is equivalent to that of a harmonically trapped noninteracting gas of particles with an effective mass (5), which in our notation is $m^* = m/(1 + \beta)$, where m is the bare-fermion mass. The mean potential energy is half of the total energy, because the gas behaves as a harmonic oscillator. Because $\beta < 0$ (6, 7), $m^* > m$, so that the effective oscillation frequencies and the chemical potential are simply scaled down, yielding $\mu_0 = k_B T_F \sqrt{1 + \beta}$ (1, 8). The total energy at zero temperature, which determines the energy scale, is therefore

$$E_0 = \frac{3}{4}N\mu_0 = \frac{3}{4}Nk_B T_F \sqrt{1 + \beta} \quad (1)$$

For each direction, the initial potential energy at zero temperature is $E_0/6$. Then, the total energy of the gas after heating is given by

$$E(t_{heat}) = \eta E_0 \left[\frac{2}{3} + \frac{1}{3}b_\perp^2 (t_{heat}) \right] \quad (2)$$

neglecting trap anharmonicity (26). Here, η is a correction factor arising from the finite temperature of the gas before the energy input. For the strongly interacting gas, the initial reduced temperature is very low. We assume that it is $\tilde{T} \approx 0.04$, where $\tilde{T}$ is measured and calibrated as described below. Assuming a Sommerfeld correction then yields $\eta_{int} \approx 1 + 2\pi^2 \tilde{T}^2/3 \approx 1.01$, which hardly affects the energy scale.

A zero-temperature strongly interacting gas expands by a hydrodynamic scale factor $b_\perp^H (t_{heat})$, when released from a harmonic trap (1, 37). Heating arises after recapture and subsequent equilibration, but not during expansion. This follows from the lowest $\tilde{T} = 0.04$, which is obtained by imaging the gas 1 ms after release from the trap. Hence, the temperature change during $t_{heat} \leq 460 \mu s < 1$ ms must be very small.

Thermometry of strongly interacting Fermi gases is not well understood. In contrast, thermometry of noninteracting Fermi gases can be simply accomplished by fitting the spatial distribution of the cloud (after release and ballistic expansion) with a Thomas-Fermi (T-F) profile, which is a function of two parameters. We choose the two parameters to be the Fermi radius σ_x and the reduced temperature T/T_F. However, this method is only precise at temperatures well below 0.5 T_F, where σ_x and T/T_F are

determined independently. At higher temperatures, where the Maxwell-Boltzmann limit is approached, such a fit determines only the product $\sigma_x^2 \times T/T_F$. We circumvent this problem by determining σ_x from a low-temperature fit, and then hold it constant in the fits at all higher temperatures, which enables a one-parameter determination of the reduced temperature.

Spatial profiles of strongly interacting Fermi gases closely resemble T-F distributions, which were observed experimentally (1, 10) and were predicted (36). The profiles of the trapped and released gas are related by hydrodynamic scaling to a good approximation. Over a wide temperature range, this scaling is consistent to ±2% with the observed cloud size and is further supported by measurements of the breathing frequency, which are within ±1% of the unitary hydrodynamic value (21). Analogous to the noninteracting case, we define an experimental dimensionless temperature parameter $\tilde{T}$, which is determined by fitting the cloud profiles with a T-F distribution holding constant the Fermi radius of the interacting gas, σ_x'. This method is inspired by the ideas presented in (38). We find experimentally that $\tilde{T}$ increases monotonically from the highly degenerate regime to the Maxwell-Boltzmann limit. This fitting procedure also leads us to define a natural reduced-temperature scale in terms of the zero-temperature parameters β and T_F,

$$\tilde{T}_{nat} \equiv \frac{k_B T}{\mu_0} = \frac{T}{T_F \sqrt{1 + \beta}} \quad (3)$$

Equation 3 is consistent with our choice of fixed Fermi radius σ_x', that is, $m\omega_x^2 \sigma_x'^2 / 2 = \mu_0$, where ω_x is the trap oscillation frequency in the x direction. At high temperatures, we must interpret $\tilde{T} = \tilde{T}_{nat}$ to obtain the correct Maxwell-Boltzmann limit. At low temperatures, $\tilde{T} \approx \tilde{T}_{nat}$ yields an estimate of T/T_F that can be further calibrated to the theoretical reduced temperature T/T_F by performing the experimental fitting procedure on the theoretically generated density profiles (26, 27).

Preliminary data processing yields normalized, one-dimensional spatial profiles of the atomic cloud (26). To determine $\tilde{T}$ over the full temperature range of interest, we used a fixed expansion time of 1 ms. We first measured σ_x' from our lowest temperature data. Then, $\tilde{T}$ was determined using the one-parameter T-F fit method. This yielded $\tilde{T}$ from 0.04 to 2.15 for the strongly interacting gas.

The experimental energy scale Eq. 1 and the natural temperature scale Eq. 3 were determined by measuring the value of β. This was accomplished by comparing the measured radius of the strongly interacting gas,

σ_x', to the radius for a noninteracting gas (26). We found that $\beta = -0.49$ (0.04) (statistical error only), which is in reasonable agreement with the best current predictions, where $\beta = -0.56$ (6) and $\beta = -0.545$ (7).

We next applied our energy input and thermometry methods to measure the heat capacity of our optically trapped Fermi gas. For different values of t_{heat}, we measured the temperature parameter $\tilde{T}$ and calculated the total energy $E(t_{heat})/E_0$ by using Eq. 2. The time t_{heat} determines the energy accurately because the trap intensity switches in less than 1 μs. We believe that shot-to-shot fluctuations in the energy are negligible, based on the small fractional fluctuations in $\tilde{T}$ at low temperatures, where the heat capacity is expected to be very small. To obtain high-resolution data, 30 to 40 different heating times t_{heat} were chosen. The data for each of these heating times were acquired in a random order to minimize systematic error. Ten complete runs were taken through the entire random sequence.

We first measured the heat capacity for a noninteracting Fermi gas (21, 26), where the scattering length a was zero. This occurred near 526 G. Figure 1 shows the data (green dots) that represent the calculated $E(t_{heat})/E_0$ versus the measured value of $\tilde{T}$, for each t_{heat}. For comparison, predictions for a noninteracting trapped Fermi gas, where $E_{ideal}(T)/E_{ideal}(0)$, are shown as the black curve, where $\tilde{T} = T/T_F$ in this case. Here, the chemical potential and energy were calculated using a finite temperature Fermi distribution and the density of states for the trapped gas. Throughout, we used the density-of-states for a realistic Gaussian potential well, $U(r) = U_0[1 - \exp(-m\overline{\omega}^2 r^2 / 2U_0)]$, where $U_0 = 14.6 k_B T_F$ and r is the radial coordinate, rather than the harmonic oscillator approximation. This model is in very good agreement with the noninteracting gas data at all temperatures.

For the strongly interacting gas at 840 G [Fig. 1 (blue diamonds)], the gas was cooled to $\tilde{T} = 0.04$ and then heated. The temperature parameter $\tilde{T}$ varies by a factor of 50, and the total energy varies by a factor of 10. For comparison, we show the theoretical results for the unitary case as the red curve. Here, the horizontal axis for the theory was obtained using the approximation $\tilde{T} \approx \tilde{T}_{nat}$ via Eq. 3. On a large-scale plot, the data for the strongly interacting and noninteracting gases appear to be quite similar, although there are important differences at low temperature.

A noticeable result is observed by plotting the low-temperature data of Fig. 1 on an expanded scale (25, 26). This reveals a transition in the heat capacity, which is made evident by plotting the data for the strongly interacting gas on a log-log scale, as in Fig. 2. The transition is apparent in the raw temperature data (25, 26) and is strongly

Fig. 1. Total energy versus temperature. For each heating time t_{heat}, the temperature parameter $\tilde{T}$ is measured from the cloud profile, and the total energy $E(t_{heat})$ is calculated from Eq. 2 in units of the ground state energy E_0. Green circles indicate noninteracting Fermi gas data and blue diamonds indicate strongly interacting Fermi gas data. The black curve shows the predicted energy versus reduced temperature for a noninteracting trapped Fermi gas, $E_{ideal}(\tilde{T})/E_{ideal}(0)$. The red curve shows the predicted energy versus $\tilde{T}$ for the unitary case. No temperature calibration is applied because $\tilde{T} \approx \tilde{T}_{nat}$ over the broad temperature range shown. Note that the lowest temperature point (blue square) is constrained to lie on the black curve.
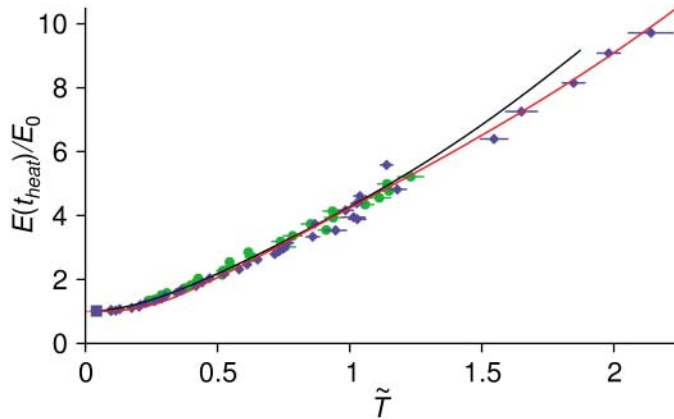
Fig. 2. Energy input versus temperature from Fig. 1 after temperature calibration on a log-log scale. The strongly interacting Fermi gas shows a transition in behavior near $T/T_F = 0.27$. Green circles indicate noninteracting Fermi gas data and blue diamonds indicate strongly interacting Fermi gas data. The red curve shows the prediction for a unitary Fermi gas in a Gaussian trap and the black curve shows the prediction for a noninteracting Fermi gas in a Gaussian trap, as in experiment. The black dashed line shows the best-fit power law [97.3 $(T/T_F)^{3.73}$] to the unitary data for $T/T_F \leq 0.27$. The inset shows the calibration curve, which has been applied to the unitary data (blue diamonds). The red dashed line in the inset represents the diagonal, $T/T_F = \sqrt{1 + \beta\tilde{T}}$. Here, $E_0 \equiv E(T=0)$.
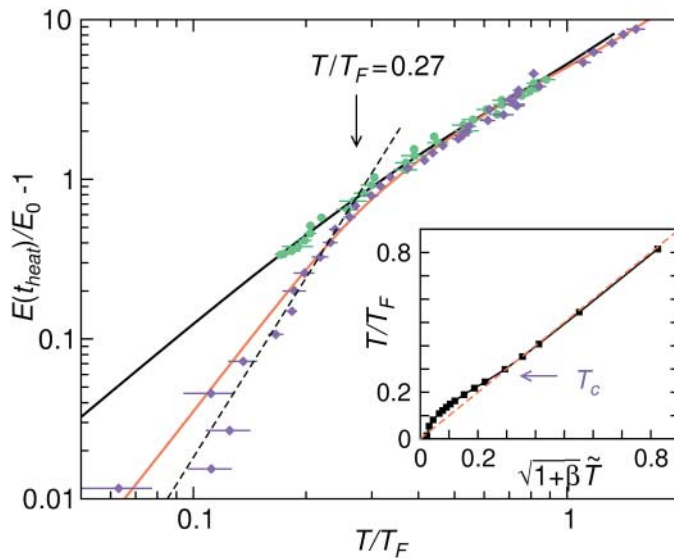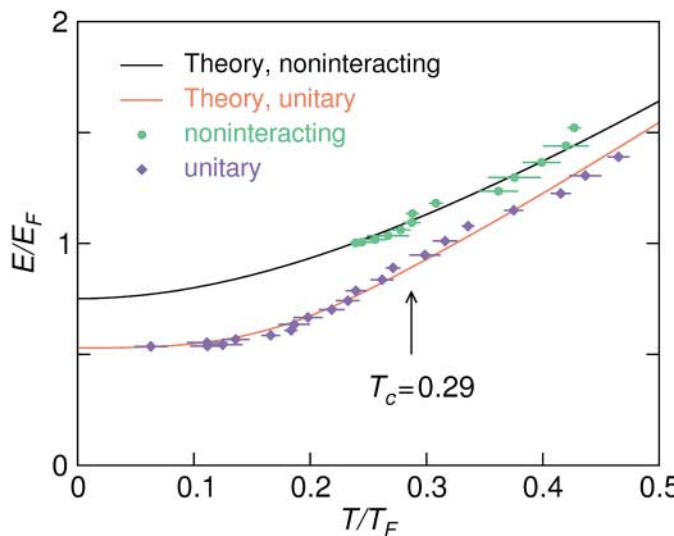
Fig. 3. Low-temperature comparison of present theory (red, black curves) and experiments (symbols) in terms of E/E_F ($E_F = k_B T_F$) per atom as a function of T/T_F, for both unitary and noninteracting gases in a Gaussian trap. The two experimental (and the two theoretical) curves do not merge until higher $T^* > T_c$, which is consistent with the presence of a pseudogap.

suggestive of the onset of superfluidity. The observed spatial profiles of the gas vary smoothly and are closely approximated by T-F shapes in the transition region. Figure 2 shows the transition after converting the empirical temperature $\tilde{T}$ to theoretical T/T_F units.

The empirical temperature was calibrated to enable precise comparison between the theory and the experimental data. For the calibration, we subjected the theoretically derived density profiles (27, 36) to the same one-dimensional T-F fitting procedure that was used in the experiments. One-dimensional density distributions were obtained by integrating over two of the three dimensions of the predicted spatial profiles, which were determined for a spherically symmetric trap. Our results for this temperature calibration are shown in the inset to Fig. 2. This calibration provides a mapping between the experimental reduced temperature $\sqrt{1 + \beta\tilde{T}}$, and the theoretical temperature T/T_F. We found that $\tilde{T} = \tilde{T}_{nat}$ is a very good approximation above T_c. Such scaling may be a manifestation of universal thermodynamics (4). The difference between $\tilde{T}$ and $\tilde{T}_{nat}$ is significant only below the superfluid transition T_c and is therefore negligible in the large-scale plot of Fig. 1 over a broad temperature range. However, below T_c, the fits to the theoretical profiles yield a value of $\sqrt{1 + \beta\tilde{T}}$, which is lower than the theoretical value of T/T_F. This is a consequence of condensate effects (26).

Figure 2 shows that above a certain temperature T_c, the strongly interacting data nearly overlap that of the noninteracting gas, and exhibit a power law fit $E/E_0 - 1 = 4.98$ $(T/T_F)^{1.43}$. Below T_c, the data deviate greatly from noninteracting Fermi gas behavior, and are well fit by $E/E_0 - 1 = 97.3$ $(T/T_F)^{3.73}$ (dashed curve). From the intersection point of these power law fits, we estimate $T_c/T_F = 0.27$ (0.02) (statistical error only). This is very close to our theoretical value $T_c/T_F = 0.29$.

The fractional change in the heat capacity C is estimated from the slope change in the fits to the calibrated data. We find the relative specific heat jump $(C_< - C_>)/C_> \approx 1.51$ (0.05) (statistical error only), where $>$ denotes above T_c and $<$ denotes below T_c. This is close to the value (1.43) for an s-wave BCS superconductor in a homogeneous case, although one expects preformed pairs, i.e., pseudogap effects, to slight modify the discontinuity (28).

In Figs. 2 and 3, the theory is compared to the calibrated data after a very slight detuning of the magnetic field in the model away from resonance, so that the predicted unitary gas parameter β has the same value as measured. This small detuning, $(k_F a)^{-1} = 0.11$, where $k_F = \sqrt{2m k_B T_F/\hbar^2}$, is reasonable given the broad Feshbach resonance (39) in ^{6}Li.

Finally, Fig. 3 presents an expanded view of the low-temperature region. Here, the experimental unitary data are calibrated and replotted in the more conventional theoretical units, $E_F = k_B T_F$ and T_F. The agreement between theory and experiment is very good. In the presence of a pseudogap, a more elaborate treatment (28) of the pseudogap self energy, which takes into account spectral broadening, will be needed in order to calculate accurately the jump in specific heat.

By extending the temperature range in Fig. 3 to high T, we find that both the unitary and noninteracting cases coincide above a characteristic temperature, T^*, although below T_c they start out with different power laws (as shown in Fig. 2). In general, we find that agreement between theory and experiment is very good over the full temperature range for which the data were taken. The observation that the interacting and noninteracting curves do not precisely coincide until temperatures rise substantially above T_c is consistent with (although it does not prove) the existence of a pseudogap and with onset temperature from the figure $T \approx 2 T_c$. Related signatures of pseudogap effects are also seen in the thermodynamics of high-temperature superconductors (17).

References and Notes

1. K. M. O'Hara, S. L. Hemmer, M. E. Gehm, S. R. Granade, J. E. Thomas, Science 298, 2179 (2002).
2. J. E. Thomas, M. E. Gehm, Am. Sci. 92, 238 (2004).
3. H. Heiselberg, Phys. Rev. A. 63, 043606 (2001).
4. T.-L. Ho, Phys. Rev. Lett. 92, 090402 (2004).
5. J. G. A. Baker, Phys. Rev. C 60, 054311 (1999).
6. J. Carlson, S.-Y. Chang, V. R. Pandharipande, K. E. Schmidt, Phys. Rev. Lett. 91, 050401 (2003).
7. A. Perali, P. Pieri, G. C. Strinati, Phys. Rev. Lett. 93, 100404 (2004).
8. M. E. Gehm, S. L. Hemmer, S. R. Granade, K. M. O'Hara, J. E. Thomas, Phys. Rev. A 68, 011401(R) (2003).
9. T. Bourdel et al., Phys. Rev. Lett. 93, 050401 (2004).
10. M. Bartenstein et al., Phys. Rev. Lett. 92, 120401 (2004).
11. M. Houbiers et al., Phys. Rev. A. 56, 4864 (1997).
12. R. Combescot, Phys. Rev. Lett. 83, 3766 (1999).
13. M. Holland, S. J. J. M. F. Kokkelmans, M. L. Chiofalo, R. Walser, Phys. Rev. Lett. 87, 120406 (2001).
14. E. Timmermans, K. Furuya, P. W. Milonni, A. K. Kerman, Phys. Lett. A 285, 228 (2001).
15. Y. Ohashi, A. Griffin, Phys. Rev. Lett. 89, 130402 (2002).
16. J. Stajic et al., Phys. Rev. A. 69, 063610 (2004).
17. Q. J. Chen, J. Stajic, S. Tan, K. Levin, available at http://arxiv.org/abs/cond-mat/0404274.
18. C. A. Regal, M. Greiner, D. S. Jin, Phys. Rev. Lett. 92, 040403 (2004).
19. M. W. Zwierlein et al., Phys. Rev. Lett. 92, 120403 (2004).
20. C. Chin et al., Science 305, 1128 (2004).
21. J. Kinast, S. L. Hemmer, M. E. Gehm, A. Turlapov, J. E. Thomas, Phys. Rev. Lett. 92, 150402 (2004).
22. M. Bartenstein et al., Phys. Rev. Lett. 92, 203201 (2004).
23. J. Kinast, A. Turlapov, J. E. Thomas, Phys. Rev. A 70, 051401(R) (2004).
24. F. London, Phys. Rev. 54, 947 (1938).
25. J. Kinast, A. Turlapov, J. E. Thomas, available at http://arxiv.org/abs/cond-mat/0409283.
26. Materials and methods are available as supporting material on Science Online.
27. Q. J. Chen, J. Stajic, K. Levin, available at http://arxiv.org/abs/cond-mat/0411090.
28. Q. J. Chen, K. Levin, I. Kosztin, Phys. Rev. B 63, 184519 (2001).
29. A. J. Leggett, Modern Trends in the Theory of Condensed Matter (Springer-Verlag, Berlin, 1980), pp. 13–27.
30. J. Kinnunen, M. Rodríguez, P. Törmä, Science 305, 1131 (2004).
31. L. D. Carr, G. V. Shlyapnikov, Y. Castin, Phys. Rev. Lett. 92, 150404 (2004).
32. J. E. Williams, N. Nygaard, C. W. Clark, N. J. Phys. 6, 123 (2004).
33. S. Stringari, Europhys. Lett. 65, 749 (2004).
34. H. Hu, A. Minguzzi, X.-J. Liu, M. P. Tosi, Phys. Rev. Lett. 93, 190403 (2004).
35. H. Heiselberg, Phys. Rev. Lett. 93, 040402 (2004).
36. J. Stajic, Q. J. Chen, K. Levin, available at http://arxiv.org/abs/cond-mat/0408104.
37. C. Menotti, P. Pedri, S. Stringari, Phys. Rev. Lett. 89, 250402 (2002).
38. B. Jackson, P. Pedri, S. Stringari, Europhys. Lett. 67, 524 (2004).
39. M. Bartenstein et al., available at http://arxiv.org/abs/cond-mat/0408673.
40. We thank T.-L. Ho, N. Nygaard, C. Chin, M. Zwierlein, M. Greiner, and D. S. Jin for stimulating correspondence. This research is supported by the Chemical Sciences, Geosciences, and Biosciences Division of the Office of Basic Energy Sciences, Office of Science, U.S. Department of Energy (DOE); the Physics Divisions of the Army Research Office; and NSF, the Fundamental Physics in Microgravity Research program of NASA, NSF-MRSEC grant DMR-0213745; and in part by the Institute for Theoretical Sciences, a joint institute of Notre Dame University and Argonne National Laboratory, and by the U.S. DOE, Office of Science through contract W-31-109-ENG-38.

Simultaneous State Measurement of Coupled Josephson Phase Qubits

R. McDermott,[1,2] R. W. Simmonds,[2] Matthias Steffen,[1] K. B. Cooper,[1] K. Cicak,[2] K. D. Osborn,[2] Seongshik Oh,[2] D. P. Pappas,[2] John M. Martinis[1]*

One of the many challenges of building a scalable quantum computer is single-shot measurement of all the quantum bits (qubits). We have used simultaneous single-shot measurement of coupled Josephson phase qubits to directly probe interaction of the qubits in the time domain. The concept of measurement crosstalk is introduced, and we show that its effects are minimized by careful adjustment of the timing of the measurements. We observe the antiphase oscillation of the two-qubit $|01\rangle$ and $|10\rangle$ states, consistent with quantum mechanical entanglement of these states, thereby opening the possibility for full characterization of multiqubit gates and elementary quantum algorithms.

Considerable progress has been made toward the implementation of a quantum computer (1) based on superconductors. Coherent single-qubit operations have been shown in Josephson flux (2) and phase (3) qubits, and the time domain interaction of coupled qubits (4) and a controlled-NOT logic gate (5) have been demonstrated in the Josephson charge qubit (6, 7). Previous studies of coupled superconducting qubits have relied on separate measurements of the individual qubits (bitwise readout). Such an approach does not yield complete information about the system and fails, for example, to directly establish correlations between the qubits in the case of an entangled state. To test quantum algorithms

efficiently or to perform quantum state tomography and thereby definitively prove entanglement, it is necessary to measure all the qubits simultaneously (wordwise readout) and with high fidelity. For multiqubit circuits with fixed coupling—a common architecture for superconducting qubits—the realization of this goal is complicated by measurement crosstalk: Measurement of the state of one qubit may perturb the state of other qubits, destroying information about quantum correlations. Although continued progress toward the realization of quantum gates in superconducting circuits requires a thorough understanding of measurement crosstalk, this issue has received little attention to date.

We describe simultaneous single-shot state measurements to probe the interaction of coupled Josephson phase qubits in the time domain. The observed antiphase oscillation of the occupation probabilities of the two-qubit basis states $|01\rangle$ and $|10\rangle$ is consistent with quantum mechanical entanglement of these

[1]Department of Physics, University of California, Santa Barbara, CA 93106, USA. [2]National Institute of Standards and Technology, 325 Broadway, Boulder, CO 80305, USA.

*To whom correspondence should be addressed. E-mail: martinis@physics.ucsb.edu